Tanzania Journal of Engineering and Technology 2024, **43**(1):1 - 13
OPEN ACCESS articles distributed under Creative Commons Attribution Licence [CC BY-ND]
Websites: https://ajol.org/tjet; https://tjet.udsm.ac.tz

ISSN 1821-536X (**print**); ISSN 2619-8789 (**electronic**)
https://doi.org/10.52339/tjet.v43i1.970

Regular Research Manuscript

Sol-gel synthesis and Microstructure Characterization of NiO-TiO_2 Semiconductor

Godlisten N. Shao

Department of Chemistry, Mkwawa University College of Education, University of Dar es Salaam
P.O. Box 2513 Iringa, Tanzania
Correspondence author email: godlisten.shao@udsm.ac.tz, shaogod@gmail.com
ORCID: https://orcid.org/0000-0001-5600-7277

ABSTRACT

NiO-TiO_2 is a fascinating p-n semiconducting binary metal oxide with unique electronic and optical properties. The NiO-TiO_2 has been synthesized using complicated preparation methods and expensive precursors that hamper their large-scale production. The present study reports the preparation of NiO-TiO_2 semiconductor with improved physicochemical properties. NiO-TiO_2 samples were prepared through one-pot sol-gel synthesis process followed by sintering of the as-synthesized materials at temperatures ranging from 600 to 1000 °C. The role of thermal treatment and NiO content on the microstructures was exquisitely studied. The microstructure of the NiO-TiO_2 samples was examined by Raman spectroscopy, XRD, XRF, SEM-EDAX, high resolution TEM, and UV-visible DRS analyses. It was revealed that the calcination temperature and the NiO content were crucial factors influenced the crystallization temperature, phase transformation, particle size and optical properties of the obtained NiO-TiO_2 systems. The incorporation of NiO in the TiO_2 microstructure generated photoactive materials with band gap energies ranging from 2.5 eV to 2.8 eV. $NiTiO_3$ system was observed in the calcined samples due to interaction of NiO and TiO_2. Therefore, in order to synthesize NiO-TiO_2 semiconductors with appealing physico-chemical properties the selection of precursors and optimization of the preparation method and calcination temperature are very important. The current study hence elucidates a facile one-pot sol-gel approach to synthesize homogeneous binary metal oxide systems with controlled morphology and crystal structure in the absence of additives.

ARTICLE INFO

Submitted: **Dec. 17, 2023**

Revised: **March 10, 2024**

Accepted: **March 26, 2024**

Published: **Apr., 2024**

Keywords: *Sol-gel process; Microstructure; Phase transformation; Nickel titanate*

INTRODUCTION

TiO_2-based metal oxides exhibit promising thermal, electrochemical and optical properties (Li *et al*., 2014, Nakata and Fujishima, 2012, Khojasteh *et al*., 2016, Pirsaheb et al., 2020, Shao et al., 2016). This enables these materials to have appreciable potential applications in sensor technology, solar cells, heterogeneous catalysis, energy storage, and biomedical technology (Shao et al., 2016, Althomali *et al*., 2023, Rahimi-

Nasrabadi et al., 2016, Ruiz-Preciado *et al*., 2015). Thus, numerous investigations have been envisaged to design versatile synthetic approaches enhancing large-scale production of TiO_2-based systems (Shao *et al*., 2013b, Shao *et al*., 2013a, Ismail and Bahnemann, 2011). Generally, TiO_2 occurs in three different polymorphic structures namely rutile, anatase or brookite phases. The polymorphs can be synthesized from various titania sources however, rutile is obtained as a result of anatase to rutile or brookite to rutile phase transformations. Consequently, the wide band gap (Eg=~3.0-3.3 eV) of TiO_2 causes a recombination of the photogenerated charge carriers that hinder its performance (Tan *et al*., 2016, Mutuma *et al*., 2015, Khojasteh et al., 2016). Nevertheless, this drawback can essentially be reduced through three strategies namely; (i) forming TiO_2 structures with mixed titania phases preferably anatase and rutile (Mutuma et al., 2015); (ii) doping of titania with non-metals (e.g. carbon, nitrogen, fluorine, or sulphur) or noble metal and transition metal (e.g. platinum, gold, cobalt, iron, vanadium, silver, or nickel); and (iii) formation of oxygen-rich TiO_2 (Shao *et al*., 2015b, Tobaldi *et al*., 2013, Tan *et al*., 2016). Thus, the above-mentioned strategies lead to improvement of the optical absorption of TiO_2 by extending its optical absorption to the visible region.

Recently, researchers have investigated the doping of TiO_2 with transition metals and rare earth elements such as La, Ni, Eu, Cu, V, W, Ce, Fe, La etc. (Ruiz-Preciado et al., 2015, Althomali *et al*., 2023, Shao *et al*., 2016). Studies have shown that the modification of TiO_2 with these elements can essentially improve its performance due to enhanced optical properties, morphology and phase structure. However, the reported materials have profoundly been fabricated using various precursors. In most studies the preparation of TiO_2 based materials requires pure titania precursors such as titanium isopropoxide or tetrabutyl orthotitanate or commercial TiO_2. Besides, various additives such as cetyltrimethylammonium bromide, polyethylene glycol, tri-block copolymer, aspartic acid, phenylalanine, amino acids, histidine, and are employed as structure-directing or capping agents (Tobaldi et al., 2013, Peña-Flores *et al*., 2014a, Rahimi-Nasrabadi *et al*., 2016). Hence, this increases the production cost and eventually limit the large-scale production of the TiO_2 based materials.

To date, versatile synthetic methods have been reported that are suitable for fabrication of the titania-based materials with promising properties for various applications. These techniques include electrospining, sol-gel, co-precipitation, spray pyrolysis, solid state reactions, hydrothermal, and chemical vapor deposition among others (Shao *et al*., 2015b, Meyer and Damonte, 2015, Althomali *et al*., 2023). Interestingly, the sol-gel process has been widely used as a result of its versatility, cost-effectiveness, simplicity, and its prospect to yield pure and homogeneous products at controllable conditions (Shao et al., 2012, Shao et al., 2016, Althomali *et al*., 2023). Thus, introducing simplified and cost-effective sol-gel process to synthesize metal oxide semiconductors from cheap sources can further enhance the large-scale production of the TiO_2 based materials.

In previous study (Shao *et al*., 2015b, Shao *et al*., 2016) it was found that doping TiO_2 with vanadium, nickel and iron yields nanostructures with improved morphology (fine and less aggregated primary particles), phase structure and optical. Among these metal oxides, NiO appears to be a more efficient system to incorporate into TiO_2 to form binary metal oxides with appealing optical properties for various applications. This is due to the fact that the ionic radius of Ni^{2+} (0.069 nm) is close to that of Ti^{4+} (0.068 nm). In addition, NiO is chemically stable and possesses high charge carrier concentration. Therefore, NiO and TiO_2

can be blended to generate metal oxides with unique properties. Interestingly, the incorporation of NiO into TiO_2 can lead to the formation of the $NiTiO_3$ system which has semiconducting and anti-ferromagnetic properties (Bañares *et al*., 1996, Ruiz-Preciado *et al*., 2015). Therefore, the present study compares the optical properties, morphology and crystal structure of NiO-TiO_2 semiconducting systems synthesized by the sol-gel in the absence of additives. A controllable, reproducible and cost-effective sol-gel process was used to synthesize NiO-TiO_2 samples. The sol-gel process suggested by the current study relies on one-pot reaction process that allows the formation of the final products with improved physico-chemical properties in the absence of additives. The reaction process allows the incorporation and homogeneous dispersion of the NiO into TiO_2. Sintering of the as-prepared samples was then performed to enhance crystallinity and phase transformation. To the best of our knowledge, only a few reports have investigated the influence of NiO in the microstructure of TiO_2 (Ruiz-Preciado et al., 2015, Althomali *et al*., 2023). Nevertheless, none of these has provided a systematic study using the preparation approach and TiO_2 precursor proposed in the present study.

METHODS AND MATERIALS

Materials

Nickel chloride hexahydrate ($NiCl_2.6H_2O$, 98%) was obtained from Yakuri Pure Chemical Co. Ltd, Japan. Ethylene glycol ($C_2H_6O_2$, 60%) was acquired from Sigma-Aldrich. Titanium oxychloride solution ($TiOCl_2$, 25 wt. %) was procured from Kukdong Chemicals Co. Ltd, Korea Republic. Ammonium hydroxide solution (28%) was purchased from Dae-Jung Chemical and Metal Co. Ltd, Korea Republic. All of the chemical reagents were obtained from commercial sources and used without further modifications.

Synthesis of the NiO-TiO2

The NiO-TiO_2 samples were prepared through a sol-gel method reported by Shao et al. (2016) with some modifications. In a typical process, 2.5 g of $NiCl_2.6H_2O$ and 2 g of $TiOCl_2$ were introduced into a beaker containing 50 mL of ethylene glycol and the solution was stirred at 25 ℃ for 2 h. Ammonium hydroxide solution was drop-wise added into the solution to pH 8-9 to yield homogeneous slurry. The temperature of the obtained slurry was raised from 25 ℃ to 80 ℃and aged under constant stirring for 6 h. After 6 h the temperature of the slurry was lowered to 25 ℃ and the product was recovered by vacuum filtration and dried at 100 ℃ for 6 h. The dried sample was thoroughly ground and then sintered in a box furnace at 600 ℃, 800 ℃ and 1000 ℃ for 2 h in an air atmosphere. The final product was dubbed NTO1 for NiO-TiO_2 whilst the sintered samples were dubbed NTOX-calcination temperature. The same experimental procedures were followed by varying the feeding weight of Ti^{4+} precursor to 1.75 g and 1.5 g to evaluate the effect of NiO in the NiO-TiO_2 samples. The final products were dubbed NTO2 and NTO_3, respectively. For the sake of comparison, pure TiO_2 powder was prepared by following procedures reported by Shao et al. (2016). The dried titania sample (TT00) was calcined at 600 ℃, 800 ℃ and 1000 ℃ to yield TT-600, TT-800 and TT-1000 samples, respectively.

Materials Characterization

The crystal structure of the prepared samples was investigated by an X-ray diffractometer (XRD-6000, Shimadzu) using Cu Kα radiation (λ=1.5406 Å). The accelerating voltage and applied current were 40 kV and 100 mA, respectively. The morphology of the samples was studied using field emission scanning electron

microscopy (FE-SEM, Hitachi S-4800 Japan) with an accelerating voltage of 15.0 kV. The energy dispersive spectroscopy (EDAX) was used to study the elemental composition and purity of the obtained samples. High-resolution transmission electron microscopy (HRTEM, Jeol JEM 2100F-Korea) was used to examine the size and distribution of the particles. Bulk elemental analysis of the samples was performed by an X-ray fluorescence spectrometer (XRF; XRF-1700, Shimadzu Co., Japan with a detection limit of 10 ppm and depth resolution of up to 10 µm). ZAF corrections (atomic number, Z) were used to determine the molar ratios of the elements present in the samples. The diffuse reflectance spectra (DRS) of the samples were recorded by a UV-visible spectrophotometer (Shimadzu, UV-2600) between 200 and 900 nm using $BaSO_4$ as a reference. The Raman spectra of the samples were recorded using a RENISHAW (RM 1000) Raman microscope with an He-Ne laser beam with wavelength of 632.8 nm.

RESULTS AND DISCUSSION

X-ray diffractograms of the samples obtained at 600, 800 and 1000 ℃ are presented in Figure 1a-d. The XRD patterns indicate that the obtained samples displayed various crystal structures depending on the calcination temperature and NiO content. Figure 1a shows that pure titania sample treated at 600 ℃ showed peaks at ~250, 380, 480 and 540-560 assignable to anatase TiO_2 crystals (Chiarello et al., 2008, Doong et al., 2009, Shao et al., 2016). On the other hand, the NiO-TiO_2 samples showed the presence of different crystal structures depending on the NiO content and calcination temperature. It can be seen that the NTO1-600 samples with 20% NiO shows the prominent peaks for $NiTiO_3$, anatase and rutile TiO_2 crystals. The peaks for the $NiTiO_3$ system can be seen at 23.90, 32.90, 35.40, 40.6, 49.30, and 57.30 while the peaks corresponding to rutile TiO2 crystals can be observed at ~27.20, 380, 480 and 540-560. The NTO2-600 with 60% NiO shows the presence of anatase TiO_2 crystals and $NiTiO_3$.

The NTO_3-600 sample with 80% NiO displayed only peaks attributable to $NiTiO_3$ and bunsenite NiO crystals. The peaks for NiO can be seen at 2Θ = 37.20 and 43.20 (El-Kemary *et al*., 2013, Ruiz-Preciado et al., 2015). Figure 1b and 1c show the XRD patterns of the samples calcined at 800 ℃ and 1000 ℃, respectively. The TT800 sample showed the presence of rutile TiO2 crystals indicating the occurrence of anatase to rutile phase transformation (ART) (Shao *et al*., 2014, Tobaldi *et al*., 2013). A complete ART was revealed in NT1-800, NT2-800, NTO1-1000, and NT2-1000 samples. It is noteworthy that the peaks for $NiTiO_3$ with increased intensity are also evidenced. The XRD results of the present study are in good agreement with literature (Khojasteh et al., 2016, Ruiz-Preciado et al., 2015). Khojasteh *et al*., (2016) found that the addition of Ni in TiO2 microstructure and eventual sintering at the calcination temperature of 700 ℃ enhances the ART and the formation of the $NiTiO_3$ phase. Generally, the $NiTiO_3$ phase is attained at higher temperatures ranging from 700 ℃ to 1350 ℃ (Ruiz-Preciado *et al*., 2015). It is noteworthy that the present study the desirable strategy to fabricate NiO-TiO_2 systems with various crystal structures through the alteration of the sintering temperature and NiO content.

The formation of the crystal structures in the calcined samples was further revealed through Raman studies. Raman spectra of TT600 and NTO1-600 sample are presented in Figure 1d as representative samples. The samples reveal Raman lines at 396, 516 and 640 cm-1 which correspond to the B1, B1g and A1g vibration modes of anatase TiO_2 crystal, respectively. Consequently, the NTO1-600 reveals Raman lines at 245-290, 345, 440, 610 and 710 cm-1 signifying the formation of the rutile TiO_2 phase. It was previously

reported that (Ruiz-Preciado *et al*., 2015) the Raman lines for $NiTiO_3$ systems are customarily found at 400-800 cm-1. Therefore, it is obvious that the Raman lines for the $NiTO_3$ phase seem to overlap with bands for rutile TiO_2 crystals thus they cannot be distinguished).

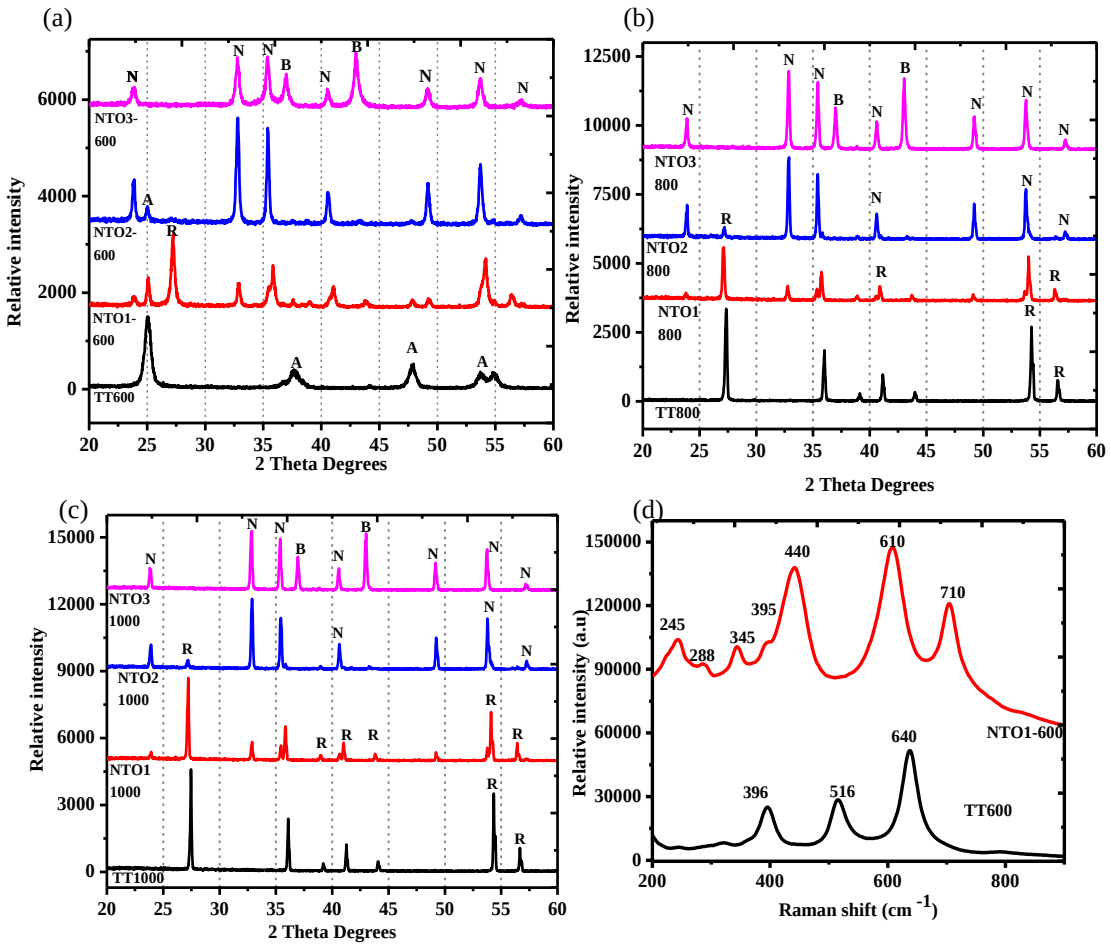

Figure 1: XRD patterns of TiO_2 and NiO_2-TiO_2 samples calcined at 600 ℃ (a) 800 ℃ (b) and 1000 ℃ (c). (d) Shows the Raman spectra of the NTO1-600 and TT600 as representative samples. The letters in the diffractograms indicates the anatase phase (A), rutile (R), $NiTiO_3$ (N), and bunsenite (B) NiO.

The interaction between Ti and Ni in the samples was examined using UV-vis diffuse reflectance spectroscopy (UV-vis DRS). The reflectance spectra were transformed to Kubelka-Munk coordinates (KM, α) and then Tauc's plots were constructed from $(KM.\ h\upsilon)^{½}$ against hυ (Shao et al., 2016). Figure 2 shows the UV-vis DRS spectra and their corresponding Tauc's plots of representative samples calcined at 600 ℃ and 800 ℃. Figure 2a reveals that pure titania sample sintered at 600 ℃ displayed a strong absorption below 415 nm associated with the ligand-to-metal charge transfer between the O^{2-} ligand and the Ti^{4+} ion (Gutiérrez *et al*., 2006, Shao *et al*., 2015a). The NTO1-600 sample shows two absorption edges located at 423 and 535 nm due to crystal field splitting caused by the $Ni^{2+}\rightarrow Ti^{4+}$ charge transfer interaction (Qu et al., 2012). NTO2-600 and NTO3-600 samples showed an absorption edge at 505 nm. The NiO-TiO_2 samples calcined at 800 ℃ (Figure 2b) show an absorption edge at 535. Thus, the NiO-TiO_2 samples

showed absorption edges extended to the visible region demonstrating that the incorporation of NiO into TiO_2 improves its optical properties (Peña-Flores *et al*., 2014b, Shao et al., 2016, El-Kemary *et al*., 2013). The indirect band gap energies were estimated by extrapolating the linear portion of the Tauc's plots onto the hυ axis. Figure 2c and 2d present the band energies (Eg) of the samples obtained at different conditions. It can be seen that the band gap of pure titania was 3.17 eV which is a normal band gap energy for anatase TiO_2 (Shao *et al*., 2015a, Ruiz-Preciado et al., 2015, El-Kemary et al., 2013). Interestingly, the band gap energies for NiO-TiO_2 samples calcined at 600 and 800°C were 2.5-2.8 eV which is relatively lower than that of anatase TiO_2. The obtained band gaps are congruent with the ones reported in literature. It was previously reported that the band gaps of NiO-TiO_2 systems can range from 2.1 eV to 3.4 eV depending on the preparation method and calcination temperature (Ruiz-Preciado *et al*., 2015, Althomali *et al*., 2023). Findings of the present study depict that photoactive NiO-TiO_2 samples were obtained which can be activated by visible light (Doong *et al*., 2009, Nair *et al*., 2012, Peña-Flores et al., 2014b).

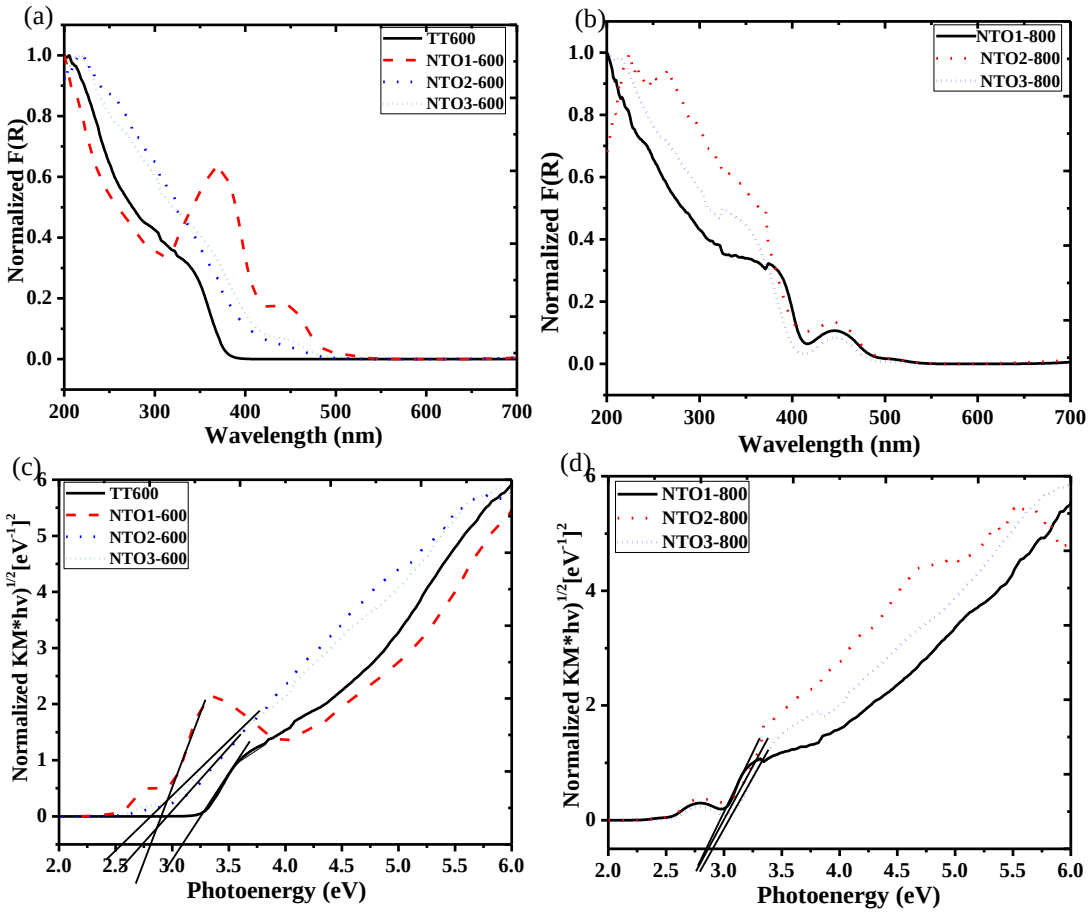

Figure 2: DRS spectra (a and b) and their respective band gaps (c and d) of the samples calcined at 600 °C and 800 °C.

The morphologies of the NiO-TiO_2 samples obtained at different conditions were examined by SEM, TEM and high resolution-TEM analyses. The EDAX results (Figure 3) indicate that the samples contained Ni, Ti and O elements as was

exemplified by the XRF results. Bulk elemental analysis of the dried powders by XRF indicated that the obtained samples had the NiO content which was approximately 20, 60 and 80%.

Figure 4a-f compile SEM micrographs of the selected representative samples sintered at 800 and 1000 ℃. It can be seen that all samples displayed porous secondary particles of different shapes. In addition, the regular secondary particles consisted of primary aggregates which are more or less spherical. Figure 4a indicates that the NTO1-800 reveals the existence of more or less rectangular shaped secondary structures whilst Figure 4b and c show that the NTO2-800 and NTO3-800 possess the rod-like secondary structures. Samples obtained at 1000 ℃ (Figure 4d, 4e and 4f) depict that the calcination of the samples at higher temperatures influenced the formation of highly porous, fine and larger primary particles.

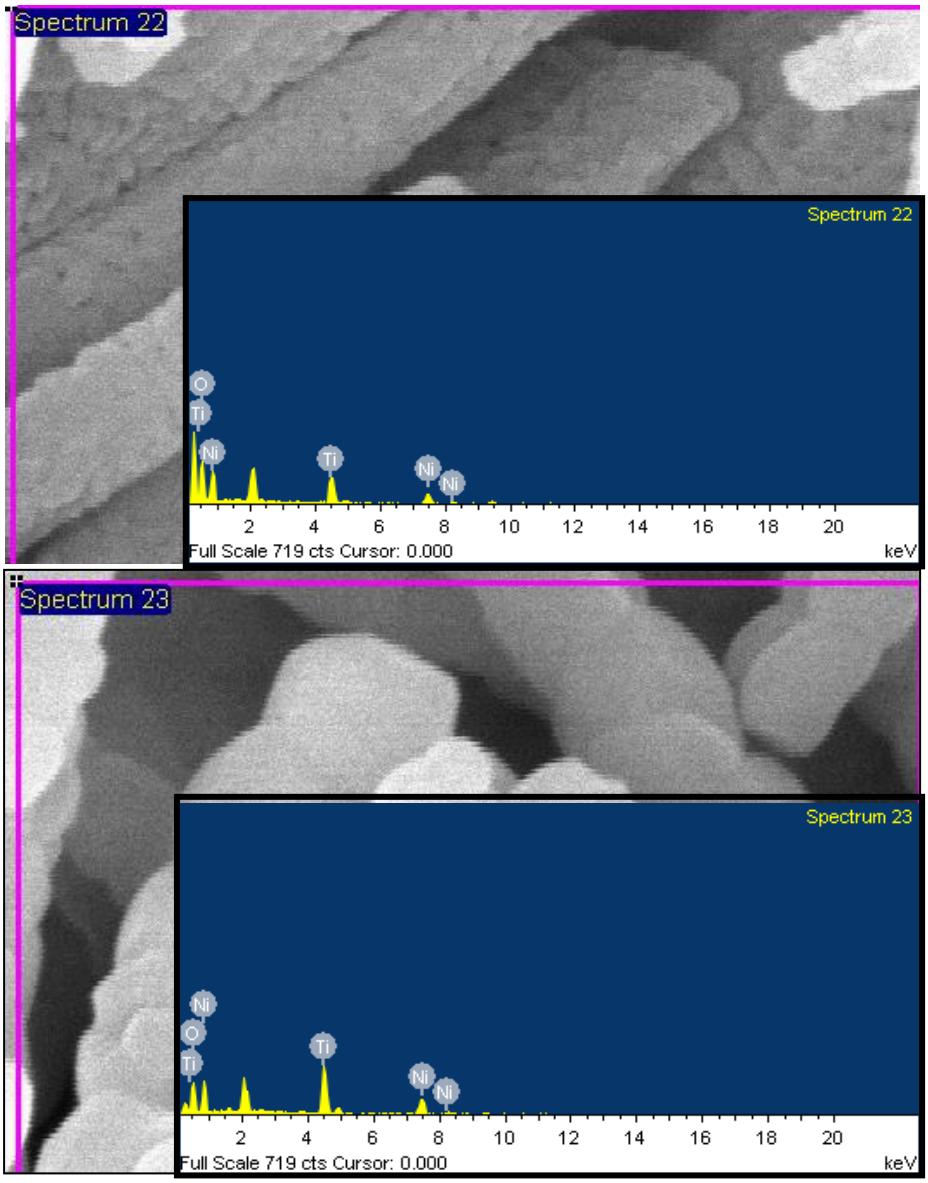

Figure 3: EDAX spectra of the NTO3-800 (a) and NTO3-1000 (b) as representative samples of the NiO-TiO_2.

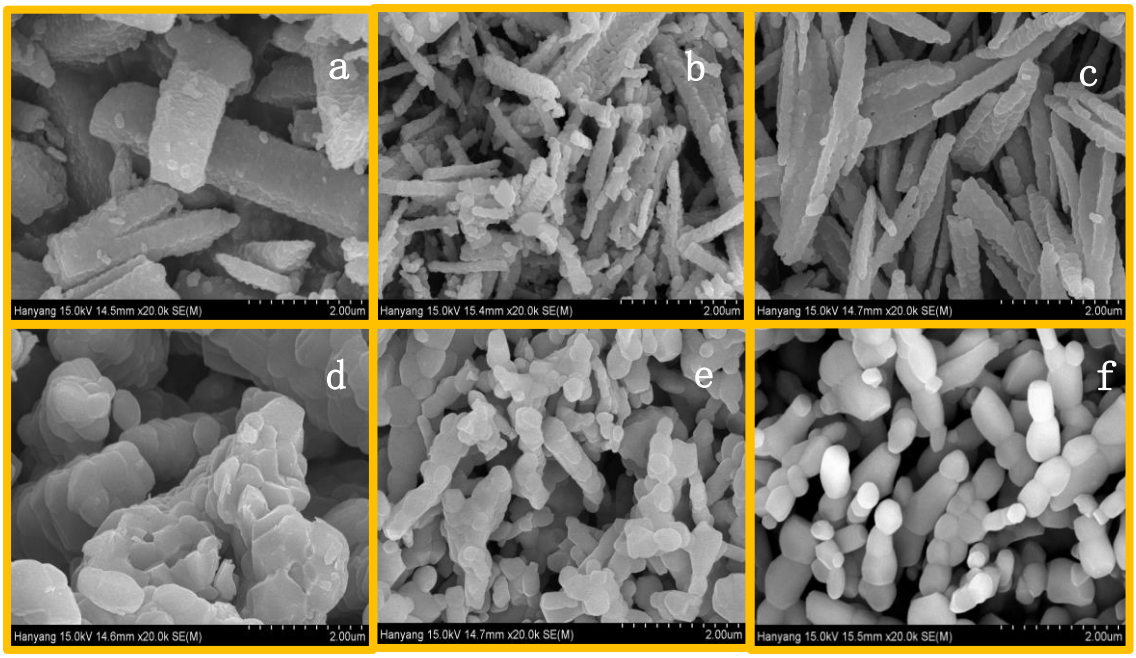

Figure 4: SEM images of NTO1-800 (a), NTO2-800 (b), NTO3-800 (c), NTO1-1000 (d), NTO2-1000 (e) and NTO3-1000 (f) as representative samples.

In order to further examine the particle size and crystalline structure of the primary particles of the NiO-TiO_2 samples, TEM and high resolution-TEM (HRTEM) analyses were employed. Figure 5 shows the TEM (Figure 5a-c) and HRTEM images (Figure 5 d-f) of the representative samples obtained at different conditions. Figure 5a-b indicates that the NTO1-600 and NTO2-600 samples exhibited primary particles with a diameter less than 100 nm. Figure 5c indicates that the NTO2-800 sample possessed regular fine particles with size ranging from 80-120 nm. Figure 5 d-f shows that the HRTEM of the NTO1-600, NTO2-600 and NTO2-800 of the prepared samples, respectively. These micrographs reveal the presence of lattice fringes corresponding the $NiTiO_3$ (0.26 nm), rutile TiO_2 (0.32 nm) and anatase TiO_2 (0.35 nm). It can be seen that the NTO1-600 showed the lattice fringes of NiTiO3, rutile TiO_2 and anatase TiO_2 indicating the formation of mixed phase NiO-TiO_2 systems. On the other hand, NTO2-600 showed the lattice fringes assignable to $NiTiO_3$ and anatase TiO_2 whilst the lattice fringes for $NiTiO_3$ and rutile TiO_2 can be seen in the NTO2-800 sample. The HRTEM results are in good agreement with the XRD results presented in Figure 1. Generally, the sol-gel method is a very suitable method for synthesizing metal oxides with improved morphology and crystal structure (Althomali *et al*., 2023). It can be suggested that the sol-gel preparation method proposed in the present study was essential in forming final products with different particle size and crystalline structure.

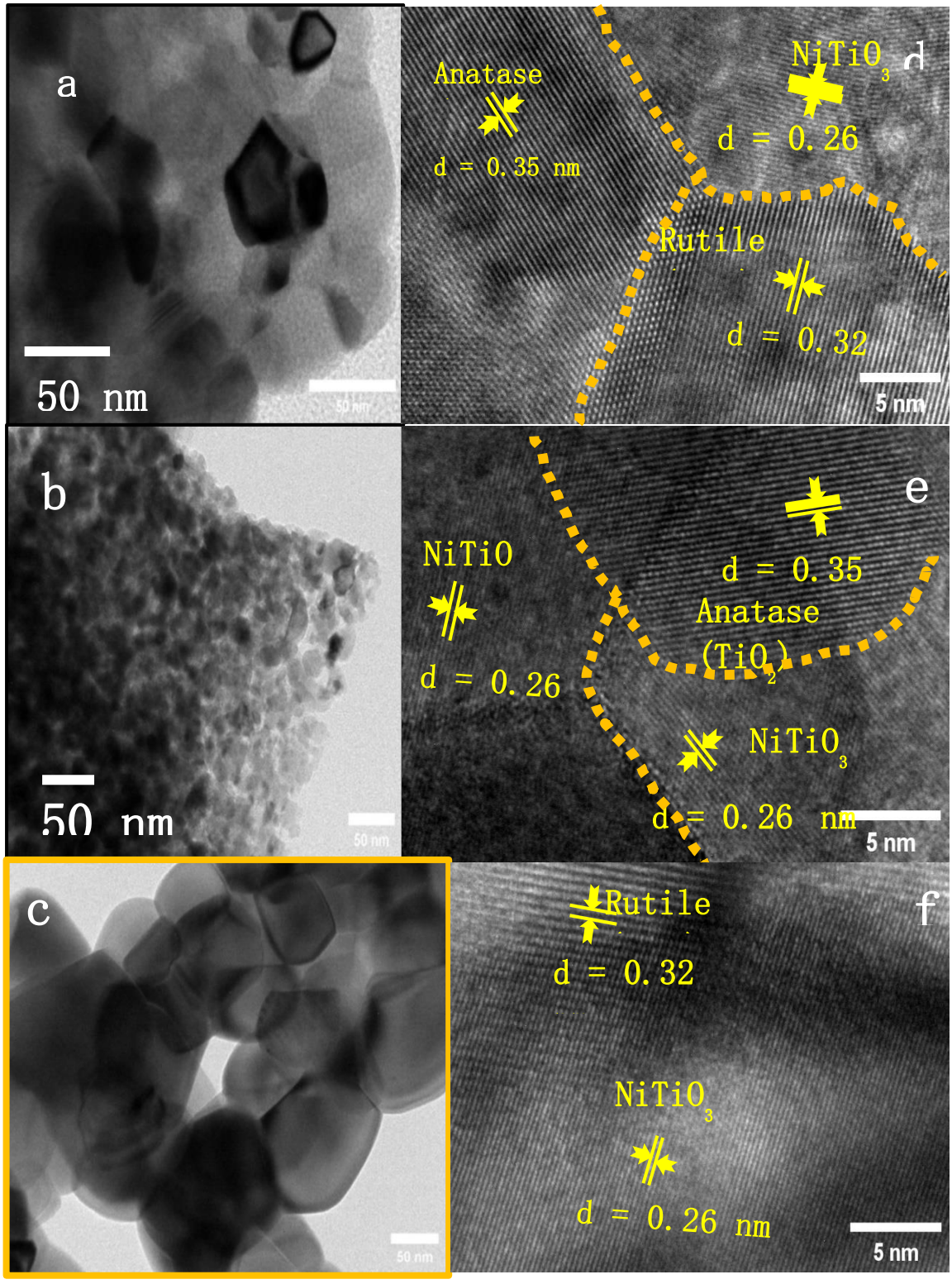

Figure 5: TEM images: NTO1-600 (a), NTO2-600 (b) and NTO2-800 (c); and HRTEM images: NTO1-600 (d), NTO2-600 (e) and NTO2-800 (f) of the NiO-TiO_2 obtained at different conditions.

The incorporation of NiO into TiO_2 system can yield binary metal oxide systems with superior physico-chemical properties. Herein, a sol-gel method was used to prepare NiO-TiO_2 systems with mixed crystal structures. Structural characterization indicated that samples with improved crystal structure, morphology and optical properties

were yielded in the absence of additives. Thus, the preparation method, NiO content and calcination temperature were very crucial in yielding final products with different physico-chemical properties. Generally, NiO-TiO_2 systems are prepared using expensive titania sources. Moreover, the interaction of NiO and TiO_2 led to the formation of the $NiTiO_3$ system after sintering of the as-prepared at calcination temperatures ranging from 600 to 1000 ℃. Various reports have shown that the $NiTiO_3$ phase can be obtained at the calcination temperatures ranging from 600 to 1350 ℃ (Ruiz-Preciado *et al*., 2015, Althomali *et al*., 2023). These findings are in good agreement with literatures however, the possibility to use facile preparation method to yield final products with superior properties is very promising and commendable.

CONCLUSION AND RECOMMENDATION

The present report introduced a controllable and convenient sol-gel approach to prepare NiO-TiO_3 systems using titanium oxychloride as a TiO_2 source in the absence of additives. Structural characterization of the final products demonstrated that samples with different physico-chemical properties can be obtained depending on the NiO content and the calcination temperature. The analysis of optical properties indicated that the incorporation of Ni^{2+} into titania produced photoactive materials as their absorption spectra were extended to the UV-visible region. XRD analysis showed samples with mixed phases were generated through varying the NiO content and sintering temperatures as well. Consequently, SEM and HRTEM analyses revealed that samples with regular and less aggregated particles were produced as well. Thus, samples exhibited superior properties (phase structure, crystallinity, morphology and porous structure) that are desirable properties for optical applications. Thus, the current study introduced the convenient method to produce TiO_2 based semiconductors with desirable properties for various applications. Therefore, one pot sol-gel process is recommended as one of the suitable preparation methods to prepare TiO_2 based semiconductors with superior properties. The preparation process can be carried out at low temperatures followed by sintering of the as-prepared materials to ensure temperature control and reproducibility. It is further anticipated that the present study will stimulate further investigations on how to prepare TiO_2 based semiconductors at lower calcination temperatures while engaging facile preparation methods and less-expensive precursors.

REFERENCES

Althomali, R. H., Jabbar, H. S., Kareem, A. T., Abdullaeva, B., Abdullaev, S. S., Alsalamy, A., Hussien, B. M., Balasim, H. M. & Mohammed, Y. 2023. Various methods for the synthesis of $NiTiO_3$ and $ZnTiO_3$ nanomaterials and their optical, sensor and photocatalyst potentials: A review. Inorganic Chemistry Communications, 111493. https://doi.org/10.1016/j.inoche.2023.111493

Bañares, M. A., Alemany, L. J., Jiménez, M. C., Larrubia, M. A., Delgado, F., López Granados, M., Martínez-Arias, A., Blasco, J. M. & Fierro, J. L. G. (1996). The role of vanadium oxide on the titania transformation under thermal treatments and surface vanadium states. Journal of Solid State Chemistry, 124, 69-76. 10.1006/jssc.1996.0209

Chiarello, G. L., Selli, E. & Forni, L., (2008). Photocatalytic hydrogen production over flame spray pyrolysis-synthesised TiO_2 and Au/TiO2. Applied Catalysis B: Environmental, 84, 332-339. http://dx.doi.org/10.1016/j.apcatb.2008.04.012

Doong, R.-A., Chang, P.-Y. & Huang, C.-H., (2009). Microstructural and photocatalytic properties of sol–gel-derived vanadium-doped

mesoporous titanium dioxide nanoparticles. Journal of Non-Crystalline Solids, 355, 2302-2308. https://doi.org/10.1016/j.jnoncrysol.2009.07.017

El-Kemary, M., Nagy, N. & El-Mehasseb, I. (2013). Nickel oxide nanoparticles: Synthesis and spectral studies of interactions with glucose. Materials Science in Semiconductor Processing, 16, 1747-1752. https://doi.org/10.1016/j.mssp.2013.05.018

Gutiérrez, O. Y., Fuentes, G. A., Salcedo, C. & Klimova, T. (2006). SBA-15 supports modified by Ti and Zr grafting for NiMo hydrodesulfurization catalysts. Catalysis Today, 116, 485-497. doi: http://dx.doi.org/10.1016/j.cattod.2006.06.035

Ismail, A. A. & Bahnemann, D. W. (2011). Mesoporous titania photocatalysts: preparation, characterization and reaction mechanisms. Journal of Materials Chemistry, 21, 11686-11707. doi: 10.1039/c1jm10407a

Khojasteh, H., Salavati-Niasari, M. & Mortazavi-Derazkola, S. (2016). Synthesis, characterization and photocatalytic properties of nickel-doped TiO_2 and nickel titanate nanoparticles. Journal of Materials Science: Materials in Electronics, 27, 3599-3607. https://doi.org/10.1007/s10854-015-4197-3

Li, Z., Ding, D., Liu, Q., Ning, C. & Wang, X. (2014). Ni-doped TiO_2 nanotubes for wide-range hydrogen sensing. Nanoscale Research Letters, 9, 118. https://doi.org/10.1186/1556-276X-9-118

Meyer, M. & Damonte, L. C. (2015). Study of Co and Fe-doped ZnO milled nanopowders. Powder Technology, 286, 371-377. http://dx.doi.org/10.1016/j.powtec.2015.07.006

Mutuma, B. K., Shao, G. N., Kim, W. D. & Kim, H. T. (2015). Sol–gel synthesis of mesoporous anatase–brookite and anatase–brookite–rutile TiO2 nanoparticles and their photocatalytic properties. Journal of Colloid and Interface Science, 442, 1-7. http://dx.doi.org/10.1016/j.jcis.2014.11.060

Nair, R. G., Roy, J. K., Samdarshi, S. K. & Mukherjee, A. K. (2012). Mixed phase V doped titania shows high photoactivity for disinfection of Escherichia coli and detoxification of phenol. Solar Energy Materials and Solar Cells, 105, 103-108. http://dx.doi.org/10.1016/j.solmat.2012.05.008

Nakata, K. & Fujishima, A. (2012). TiO_2 photocatalysis: Design and applications. Journal of Photochemistry and Photobiology C: Photochemistry Reviews, 13, 169-189. http://dx.doi.org/10.1016/j.jphotochemrev.2012.06.001

Peña-Flores, J. I., Palomec-Garfias, A. F., Márquez-Beltrán, C., Sánchez-Mora, E., Gómez-Barojas, E. & Pérez-Rodríguez, F. (2014a). Fe effect on the optical properties of TiO_2:Fe_2O_3 nanostructured composites supported on SiO_2 microsphere assemblies. Nanoscale research letters, 9, 1-7. https://doi.org/10.1186/1556-276X-9-499

Peña-Flores, J. I., Palomec-Garfias, A. F., Márquez-Beltrán, C., Sánchez-Mora, E., Gómez-Barojas, E. & Pérez-Rodríguez, F. (2014b). Fe effect on the optical properties of TiO_2:Fe_2O_3 nanostructured composites supported on SiO_2 microsphere assemblies. Nanoscale Research Letters, 9, 499-499. 10.1186/1556-276X-9-499

Pirsaheb, M., Hossaini, H., Nasseri, S., Azizi, N., Shahmoradi, B. & Khosravi, T. (2020). Optimization of photocatalytic degradation of methyl orange using immobilized scoria-Ni/TiO_2 nanoparticles. Journal of Nanostructure in Chemistry, 10, 143-159. https://doi.org/10.1007/s40097-020-00337-x

Qu, Y., Zhou, W., Ren, Z., Du, S., Meng, X., Tian, G., Pan, K., Wang, G. & Fu, H., (2012). Facile preparation of porous $NiTiO_3$ nanorods with enhanced visible-light-driven photocatalytic performance. Journal of Materials Chemistry, 22, 16471-16476. 10.1039/C2JM32044D

Rahimi-Nasrabadi, M., Ahmadi, F. & Eghbali-Arani, M., (2016). Novel route to synthesize nanocrystalline nickel titanate in the presence of amino acids as a capping agent. Journal of Materials Science: Materials in Electronics, 27, 11873-11878. https://doi.org/10.1007/s10854-016-5331-6

Ruiz-Preciado, M. A., Kassiba, A., Gibaud, A. & Morales-Acevedo, A., (2015). Comparison of nickel titanate ($NiTiO_3$) powders synthesized by sol–gel and solid state reaction. Materials Science in Semiconductor Processing, 37, 171-178. https://doi.org/10.1016/j.mssp.2015.02.063

Shao, G. N., Elineema, G., Quang, D. V., Kim, Y. N., Shim, Y. H., Hilonga, A., Kim, J.-K. & Kim, H. T., (2012). Two step synthesis of a mesoporous titania–silica composite from titanium oxychloride and sodium silicate. Powder Technology, 217, 489-496. http://dx.doi.org/10.1016/j.powtec.2011.11.008

Shao, G. N., Engole, M., Imran, S. M., Jeon, S. J. & Kim, H. T., (2015a). Sol–gel synthesis of photoactive kaolinite-titania: Effect of the preparation method and their photocatalytic properties. Applied Surface Science, 331, 98-107. http://dx.doi.org/10.1016/j.apsusc.2014.12.199

Shao, G. N., Hilonga, A., Jeon, S. J., Lee, J. E., Elineema, G., Quang, D. V., Kim, J.-K. & Kim, H. T., (2013a). Influence of titania content on the mesostructure of titania–silica composites and their photocatalytic activity. Powder Technology, 233, 123-130. http://dx.doi.org/10.1016/j.powtec.2012.08.025

Shao, G. N., Imran, S. M., Jeon, S. J., Engole, M., Abbas, N., Haider, S. M., Kang, S. J. & Kim, H. T., (2014). Sol–gel synthesis of photoactive zirconia–titania from metal salts and investigation of their photocatalytic properties in the photodegradation of methylene blue. Powder Technology, 258, 99-109. http://dx.doi.org/10.1016/j.powtec.2014.03.024

Shao, G. N., Imran, S. M., Jeon, S. J., Kang, S. J., Haider, S. M. & Kim, H. T., (2015b). Sol–gel synthesis of vanadium doped titania: Effect of the synthetic routes and investigation of their photocatalytic properties in the presence of natural sunlight. Applied Surface Science, 351, 1213-1223. http://dx.doi.org/10.1016/j.apsusc.2015.06.047

Shao, G. N., Jeon, S.-J., Haider, M. S., Abbass, N. & Kim, H. T., (2016). Investigation of the influence of vanadium, iron and nickel dopants on the morphology, and crystal structure and photocatalytic properties of titanium dioxide based nanopowders. Journal of Colloid and Interface Science, 474, 179-189. http://dx.doi.org/10.1016/j.jcis.2016.04.024

Shao, G. N., Kim, Y., Imran, S. M., Jeon, S. J., Sarawade, P. B., Hilonga, A., Kim, J.-K. & Kim, H. T. (2013b). Enhancement of porosity of sodium silicate and titanium oxychloride based TiO_2–SiO_2 systems synthesized by sol–gel process and their photocatalytic activity. Microporous and Mesoporous Materials, 179, 111-121. http://dx.doi.org/10.1016/j.micromeso.2013.05.021

Tan, L.L., Ong, W.J., Chai, S.P. & Mohamed, A. R. (2016). Visible-light-activated oxygen-rich TiO_2 as next generation photocatalyst: Importance of annealing

temperature on the photoactivity toward reduction of carbon dioxide. Chemical Engineering Journal, 283, 1254-1263. https://doi.org/10.1016/j.cej.2015.07.093

Tobaldi, D. M., Sever Škapin, A., Pullar, R. C., Seabra, M. P. & Labrincha, J. A. (2013). Titanium dioxide modified with transition metals and rare earth elements: Phase composition, optical properties, and photocatalytic activity. Ceramics International, 39, 2619-2629. http://dx.doi.org/10.1016/j.ceramint.2012.09.027